Character of the structural and magnetic phase transitions in the parent and electron-doped BaFe_{2}As_{2} compounds

M. G. Kim, R. M. Fernandes, A. Kreyssig, J. W. Kim, A. Thaler, S. L. Bud'ko, P. C. Canfield, R. J. McQueeney, J. Schmalian, and A. I. Goldman

Phys. Rev. B **83**, 134522 — Published 28 April 2011

DOI: 10.1103/PhysRevB.83.134522

Character of the structural and magnetic phase transitions in the parent and electron doped $BaFe_2As_2$ compounds

M. G. Kim[1], R. M. Fernandes[1], A. Kreyssig[1], J. W. Kim[2], A. Thaler[1], S. L. Bud'ko[1], P. C. Canfield[1], R. J. McQueeney[1], J. Schmalian[1] and A. I. Goldman[1]
[1]*Ames Laboratory, U.S. DOE and Department of Physics and Astronomy Iowa State University, Ames, IA 50011, USA and*
[2]*Advanced Photon Source, Argonne National Laboratory, Argonne, Illinois 60439, USA*

We present a combined high-resolution x-ray diffraction and x-ray resonant magnetic scattering (XRMS) study of as-grown $BaFe_2As_2$. The structural/magnetic transitions must be described as a two-step process. At T_S = 134.5 K we observe the onset of a second-order structural transition from the high-temperature paramagnetic tetragonal structure to a paramagnetic orthorhombic phase, followed by a discontinuous step in the structural order parameter that is coincident with a first-order antiferromagnetic (AFM) transition at T_N = 133.75 K. These data, together with detailed high-resolution x-ray studies of the structural transition in lightly doped $Ba(Fe_{1-x}Co_x)_2As_2$ and $Ba(Fe_{1-x}Rh_x)_2As_2$ compounds, show that the structural and AFM transitions do, in fact, occur at slightly different temperatures in the parent $BaFe_2As_2$ compound, and evolve towards split second-order transitions as the doping concentration is increased. We estimate the composition for the tricritical point for Co-doping and employ a mean-field approach to show that our measurements can be explained by the inclusion of an anharmonic term in the elastic free energy and magneto-elastic coupling in the form of an emergent Ising-nematic degree of freedom.

PACS numbers: 74.70.Xa, 75.25.+z, 75.40.Cx, 75.50.Ee

I. INTRODUCTION

Although most of the excitement surrounding the discovery[1,2] of superconductivity (SC) in the iron pnictide compounds has focused on the underlying mechanism, these compounds also provide us with a fascinating opportunity to study subtle, and not so subtle, aspects of the interactions between SC, structure and magnetism. A great deal of this research has focused on the *R*FeAsO (*R* = rare earth), or *1111* compounds, and the *AE*Fe_2As_2 (*AE* = alkaline earth), or *122* family. The parent *1111* and *122* systems undergo transitions from a high-temperature paramagnetic (PM) tetragonal phase to a low-temperature antiferromagnetic (AFM) orthorhombic structure.[3–9] In the *1111* parent compounds, the structural transition occurs at somewhat higher temperature than the AFM ordering.[3] In the *122* parent compounds, these transitions appear coincident in temperature and coupled.[5,7–9]

The consequences of electron/hole doping for the $BaFe_2As_2$ compound have been studied widely. For example, upon electron doping through substitution on the Fe site by Co, Ni, Rh, Pt or Pd, the structural and AFM transitions are suppressed and split, with the structural transition found at somewhat higher temperature.[10–18] Superconductivity emerges over a small but finite range in dopant concentration. In contrast, the structural and AFM transitions remain coincident in superconducting samples produced by K doping on the Ba site, P doping on the As site, and Ru doping on the Fe site.[2,19–22] In Co-, Rh-, Ni-, and Ru-doped $BaFe_2As_2$, neutron and x-ray measurements revealed a suppression in both the magnetic order parameter and the orthorhombic distortion below the superconducting transition temperature, which indicates the coexistence and competition between magnetism and superconductivity in these systems.[15–18,22–24]

The nature of the structural and AFM transitions has, itself, been the subject of intense scrutiny. For $CaFe_2As_2$ and $SrFe_2As_2$, several neutron, x-ray, μSR and NMR measurements have reported that the structural/magnetic transitions are discontinuous (first-order) and hysteretic.[5–8,25] However, in $BaFe_2As_2$, there has been significant debate concerning the character of the structural and magnetic order parameters. Early neutron measurements on polycrystalline samples found a second-order magnetic transition.[9] Neutron diffraction measurements by some groups, however, described a first-order magnetic transition but failed to observe any hysteresis,[26] while neutron and NMR measurements by others found a first-order magnetic transition and observed a large hysteresis upon cooling and warming.[27,28] Wilson *et al.* initially reported that the magnetic and structural transitions in $BaFe_2As_2$ were continuous in nature, and could be described by a simple power-law dependence with an critical exponent consistent with a two-dimensional Ising model.[29,30] Later heat capacity and x-ray work by this group on annealed samples of $BaFe_2As_2$ found that the orthorhombic distortion appeared first as a second-order transition interrupted, at slightly lower temperature, by a first-order transition to the low temperature orthorhombic phase.[31] As noted by these authors, this complex structural transition and its relationship to the concomitant AFM ordering calls for further investigations.

To shed light on the nature of structural and magnetic transitions, we present a combined high-resolution x-ray diffraction and x-ray resonant magnetic scattering (XRMS) study of as-grown $BaFe_2As_2$. In Section II we provide details of the scattering experiments on the parent $BaFe_2As_2$ compound and the Co- and Rh-doped compounds. In Sections III, we report the results of high-resolution x-ray diffraction and XRMS measurements on the parent $BaFe_2As_2$ compound and show that there is a small, but distinct, difference in the temperatures of the structural and AFM transitions. We also studied the doped compounds to substantiate our conclusion that the structural transition is continuous in nature, whereas the AFM transi-

tion changes from a first-order transition at low doping to a second-order transition for higher doping levels as the system passes through a tricritical point. In Section IV, we estimate the position of this tricritical point for the $Ba(Fe_{1-x}Co_x)_2As_2$ phase diagram and employ a mean-field approach to show that our measurements can be explained by the inclusion of an anharmonic term in the elastic free energy and magneto-elastic coupling in the form of an emergent Ising-nematic degree of freedom. In Section V, we summarize our results.

II. EXPERIMENTAL DETAILS

Single crystals of $BaFe_2As_2$, $Ba(Fe_{1-x}Co_x)_2As_2$ and $Ba(Fe_{1-x}Rh_x)_2As_2$ compounds were produced using the self-flux solution growth method described elsewhere.[11] Energy dispersive spectroscopy (EDS) was performed to confirm the absence of foreign elements, and wavelength dispersive spectroscopy (WDS) was employed to determine the compositions of the Co- and Rh-doped compounds at several points on each sample, providing a combined statistical and systematic error of less than 5% of the relative elemental concentration [e.g. 0.018 ± 0.001 for the $Ba(Fe_{0.982}Co_{0.018})_2As_2$ sample]. Temperature-dependent ac electrical resistance data (f = 16 Hz, I = 3 mA) were collected using a Quantum Design Magnetic Properties Measurement System (MPMS) with a Linear Research LR700 resistance bridge. Electrical contact was made to the sample using Epotek H20E silver epoxy to attach Pt wires in a four-probe configuration.

Temperature-dependent, high-resolution, single-crystal x-ray diffraction measurements were performed on a four-circle diffractometer using Cu $K_{\alpha1}$ radiation from a rotating anode x-ray source, selected by a germanium (1 1 1) monochromator. For these measurements, the plate-like single crystals with typical dimensions of $3 \times 3 \times 0.5\,\mathrm{mm}^3$ were attached to a flat copper sample holder on the cold finger of a closed-cycle displex refrigerator. The mosaicities of the $BaFe_2As_2$, $Ba(Fe_{1-x}Co_x)_2As_2$ and $Ba(Fe_{1-x}Rh_x)_2As_2$ single crystals were all less than 0.02° full-width-at-half-maximum (FWHM) as measured by the rocking curves of the (1 1 10) reflection at room temperature. The diffraction data were obtained as a function of temperature between room temperature and 8 K, the base temperature of the refrigerator.

To correlate the evolution of the structure with the occurrence of magnetic order, both conventional x-ray diffraction and XRMS measurements were performed on the 6ID-B beamline at the Advanced Photon Source (APS) using the same as-grown $BaFe_2As_2$ single crystal studied with the laboratory source. The single crystal was attached to a flat copper sample holder on the cold finger of a closed-cycle displex refrigerator with the tetragonal (HHL) plane coincident with the vertical scattering plane. The temperature, measured at a sensor mounted to the copper block holding the sample, was stable within ±0.002 K. Care was taken to ensure that heating effects associated with the incident x-ray beam were minimized by measuring charge and magnetic reflections in close proximity and using the appropriate incident beam attenuation. Measurements of both the charge scattering and the XRMS were done at the Fe K-edge (E = 7.112 keV).[32] The incident radiation was linearly polarized perpendicular to the vertical scattering plane (σ-polarized) with a spatial cross section of 1.0 mm (horizontal) × 0.2 mm (vertical). In this configuration, dipole resonant magnetic scattering rotates the plane of linear polarization into the scattering plane (π-polarization), while the charge scattering leaves the polarization unchanged. Cu (2 2 0) was used as a polarization analyzer to suppress the charge and fluorescence background relative to the magnetic scattering signal by approximately a factor of 200.

III. RESULTS

A. High-resolution x-ray diffraction and XRMS measurements of $BaFe_2As_2$

In Fig. 1(a), we display [ξ ξ 0] scans through the $(1\ 1\ 10)_T$ charge peak, obtained using the laboratory source, for the parent $BaFe_2As_2$ compound measured with temperature steps of 0.25 K. Above the structural transition temperature, T_S = 134.5 K, we observe a single sharp peak consistent with the tetragonal structure. Upon cooling below T_S, the $(1\ 1\ 10)_T$ charge peak continuously broadens and, then, clearly splits at T = 133.75 K concomitant with the abrupt appearance of two additional peaks at this temperature [vertical arrows in Fig. 1(a)] bracketing the two inner peaks. Upon further cooling, the splitting of the two inner peaks evolves continuously as their intensities decrease, whereas the positions of the outer peaks change only slowly as their intensities increase. Below T = 133.0 K, the two inner peaks disappeared leaving only the outer peaks in evidence. We note that these observations are qualitatively consistent with similar diffraction measurements on an annealed sample of $BaFe_2As_2$ recently reported by Rotundu *et al*.[31] although the transition temperatures for their annealed sample were approximately 5 K higher.

Having described the temperature evolution of the diffraction peaks qualitatively, it is useful at this point to introduce some labeling of the corresponding phases. The high-temperature paramagnetic phase is denoted as Tet-PM. Anticipating the results of our XRMS study, we label the orthorhombic phase that evolves continuously over a very narrow temperature range below T_S [corresponding to the inner pair of peaks in Fig. 1(a)] as Ort-PM. We further label the orthorhombic phase that abruptly appears at T = 133.75 K [corresponding to the two outer bracketing peaks in Fig. 1(a)] as Ort-AFM. Structurally, we assume that Ort-PM and Ort-AFM differ only with respect to the values of their lattice constants and orthorhombic distortion at a given temperature.

Figure 1(b) describes the temperature evolution of these phases. Upon cooling, a second-order transition from Tet-PM to Ort-PM occurs at T_S = 134.5 K followed by a first-order transition to Ort-AFM at T_N = 133.75 K. There is a region of coexistence between Ort-AFM and Ort-PM from 133.75 K to 133.0 K, and only the Ort-AFM phase is observed below this temperature. Upon warming, Ort-PM appears at 133.0 K and coexists with Ort-AFM up to T_N' = 134.0 K, where Ort-AFM

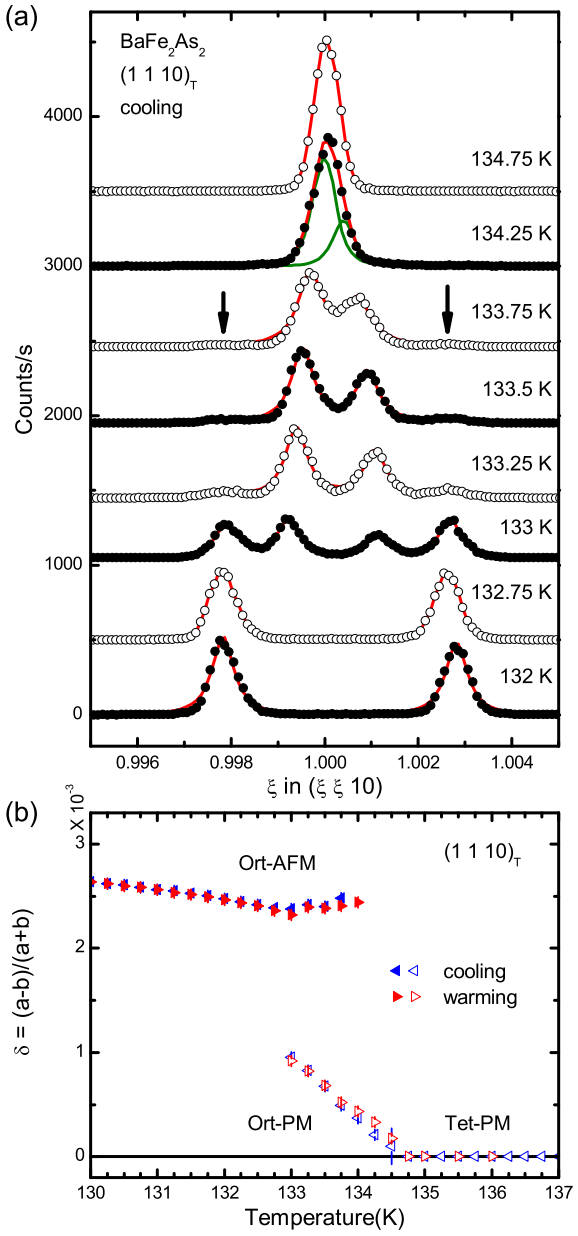

FIG. 1: (Color online) (a) X-ray diffraction scans, measured using the laboratory source, along the [ξ ξ 0] direction through the position of the tetragonal (1 1 10)$_T$ reflection for selected temperatures in the parent $BaFe_2As_2$ upon cooling. The lines present the fitted curves using a Lorentzian-squared line shape. The two-component fit to broadened peaks is illustrated for T = 134.25 K. The arrows denote the positions of peaks associated with Ort-AFM as discussed in the text. At this temperature, the integrated intensity of the Ort-AFM peaks are approximately 5% of the Ort-PM diffraction peaks. (b) The orthorhombic distortion as a function of temperature upon cooling and warming determined from fits to the (1 1 10) Bragg diffraction peak.

disappears. The orthorhombic distortion associated with Ort-PM decreases continuously up to T_S = 134.5 K, where Tet-PM is recovered. We find no hysteresis in the transformations from Tet-PM to Ort-PM and $\lesssim$0.25 K hysteresis associated with the appearance/disappearance of Ort-AFM.

In order to investigate the relationship between the structural transition and AFM ordering in this system we have performed a combined study using high-resolution x-ray diffraction and XRMS measurements. These simultaneous measurements eliminate concerns regarding disparities in the temperature calibration of sensors for different experiments. Using the configuration at the APS described in the last section we measured the scattering at both the charge and magnetic Bragg peak positions for several temperatures close to the structural transition. In Fig. 2(a) we show a [ξ ξ 0] scan through the (1 1 8)$_T$ charge Bragg peak at T = 137 K, well above the structural transition temperature. At T = 130 K, below T_N and T_S, two well-separated peaks were observed [Fig. 2(b)]. These are the (2 0 8)$_O$ and (0 2 8)$_O$ charge Bragg peaks of the orthorhombic phase. The difference in intensity arises from different populations of the domains within the illuminated volume of the sample. At this same temperature, a single peak is found at the (1 0 7)$_O$, magnetic peak position for the orthorhombic phase, [Fig. 2(c)] in agreement with previous measurements of a magnetic propagations vector given by $\mathbf{Q}_m$ = (1 0 1)$_O$ [($\frac{1}{2}$ $\frac{1}{2}$ 1)$_T$] with lattice constants $a_O > b_O$.[9,26,27,29,32] For simplicity, we will henceforth label all peaks with tetragonal indices. Therefore, the (1 0 7)$_O$ magnetic Bragg peak will be referred to as ($\frac{1}{2}$ $\frac{1}{2}$ 7)$_T$, keeping in mind that the magnetic peaks are displaced from $\xi = \frac{1}{2}$ because of the orthorhombic distortion.

The principal result conveyed in Figs. 2(b) and (c) is that the expected AFM order exists in the Ort-AFM phase. The question, however, is whether this AFM order is also associated with the Ort-PM intermediate phase. Figures 2(d) and (e) show [ξ ξ 0] scans through the (1 1 8)$_T$ charge and ($\frac{1}{2}$ $\frac{1}{2}$ 7)$_T$ magnetic peak positions at T = 133.3 K. Similar to what was found in our laboratory-based measurement [Fig. 1(a)] we observed four charge peaks [two outer peaks from Ort-AFM and two inner peaks from Ort-PM]. However, Fig. 2(e) displays only a single magnetic peak. The arrows in this panel denote the expected positions for magnetic peaks associated with each of the charge peaks in Fig. 2(d) and we see that the magnetic peak is found at a position that corresponds to one of the two outer peaks associated with the Ort-AFM phase. This allows us to conclude that the magnetic order is associated only with the Ort-AFM phase. Taken together, the x-ray diffraction and XRMS measurements suggest that: (1) The orthorhombic distortion at T_S is best described as a second-order transition; (2) the structural and AFM transitions in the as-grown $BaFe_2As_2$ compound are separated in temperature by approximately 0.75 K and; (3) a first-order magnetic transition at T_N drives the discontinuity in the structural order parameter at 133.75 K. To further substantiate these conclusions, we now turn to a study of the evolution of the structural transition in electron-doped $BaFe_2As_2$ compounds.

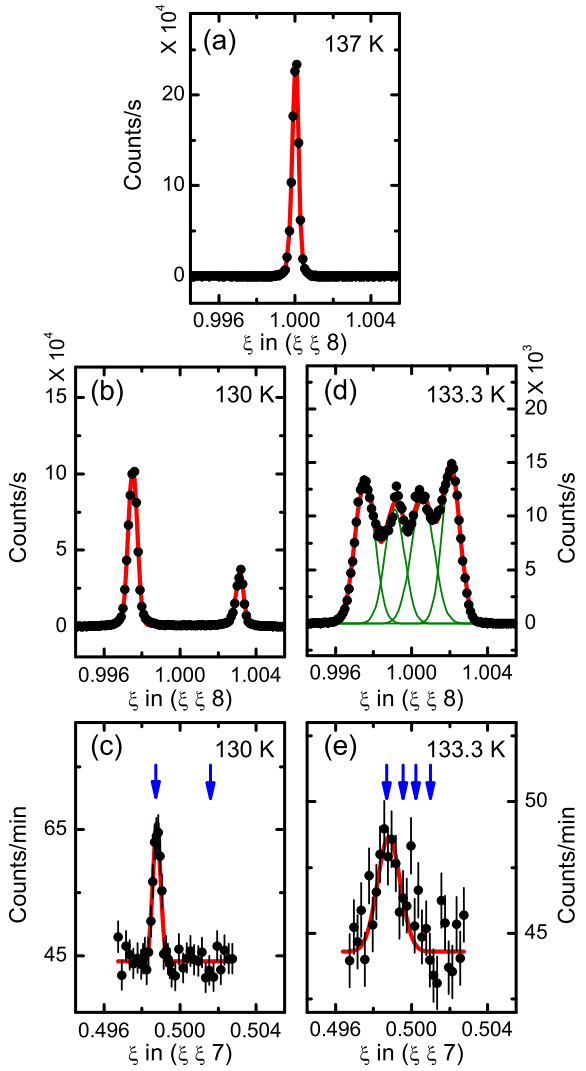

FIG. 2: (Color online) (a) The measured (1 1 8)$_T$ charge diffraction peak above the structural/magnetic transitions. Panels (b) and (c) show the (1 1 8)$_T$ charge peak and ($\frac{1}{2}$ $\frac{1}{2}$ 7)$_T$ magnetic peak at T = 130 K, well below the transition region. Panels (d) and (e) show the measured intensities at the (1 1 8)$_T$ charge peak and ($\frac{1}{2}$ $\frac{1}{2}$ 7)$_T$ magnetic positions at T = 133.3 K. The arrows in (c) and (e) indicate the calculated magnetic peak positions corresponding to each of the charge peaks in (b) and (d), respectively. The fitted value for the width of the charge and magnetic peaks are the same.

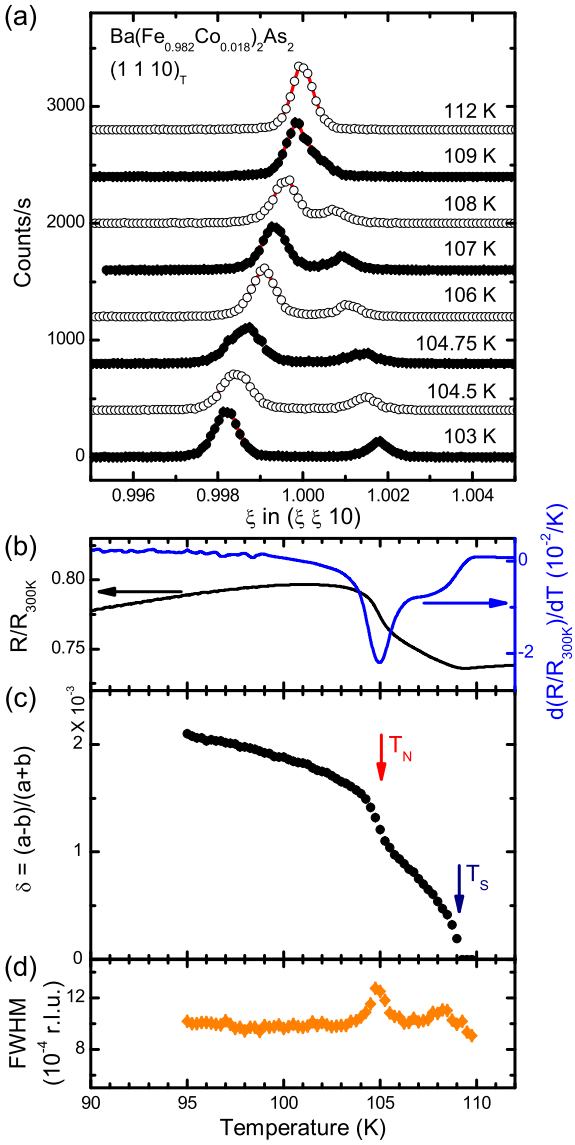

FIG. 3: (Color online) (a) X-ray data, (b) resistance (black line) and its temperature derivative (blue line), (c) orthorhombic distortion and (d) FWHM of the split (1 1 10)$_T$ Bragg peaks measured for Ba(Fe$_{1-x}$Co$_x$)$_2$As$_2$ with x = 0.018. In panel (c) the structural and magnetic transition temperatures are marked.

B. High-resolution x-ray diffraction and resistance measurements of Ba(Fe$_{1-x}$Co$_x$)$_2$As$_2$ and Ba(Fe$_{1-x}$Rh$_x$)$_2$As$_2$

It has already been established that the substitution of Co or Rh for Fe in the parent $BaFe_2As_2$ compound results in new and interesting behavior.[10–12,14–17,23,24] As doping is increased, both the structural and magnetic transitions are suppressed and split, with the structural transition occurring at higher temperature. In Ba(Fe$_{1-x}$Co$_x$)$_2$As$_2$, for Co concentrations $0.03 \leq x \leq 0.06$, we enter a region of the phase diagram where magnetism and superconductivity coexist and compete.[11,24] Within this region, the magnetic and structural transitions are well-separated in temperature, and continuous in nature (see for example, references 23 and 24). It is, therefore, interesting to probe the behavior of the structural and AFM transitions, described above, as they evolve towards split second-order transitions with doping.

To this end, we have performed high-resolution x-ray diffraction measurements on four doped $BaFe_2As_2$ samples: Ba(Fe$_{1-x}$Co$_x$)$_2$As$_2$ for x = 0.018 and 0.047, and Ba(Fe$_{1-x}$Rh$_x$)$_2$As$_2$ for x = 0.012 and 0.040. Figures 3 through 6 display the raw diffraction data, the orthorhombic distortion (δ) and diffraction peak widths derived from fits to

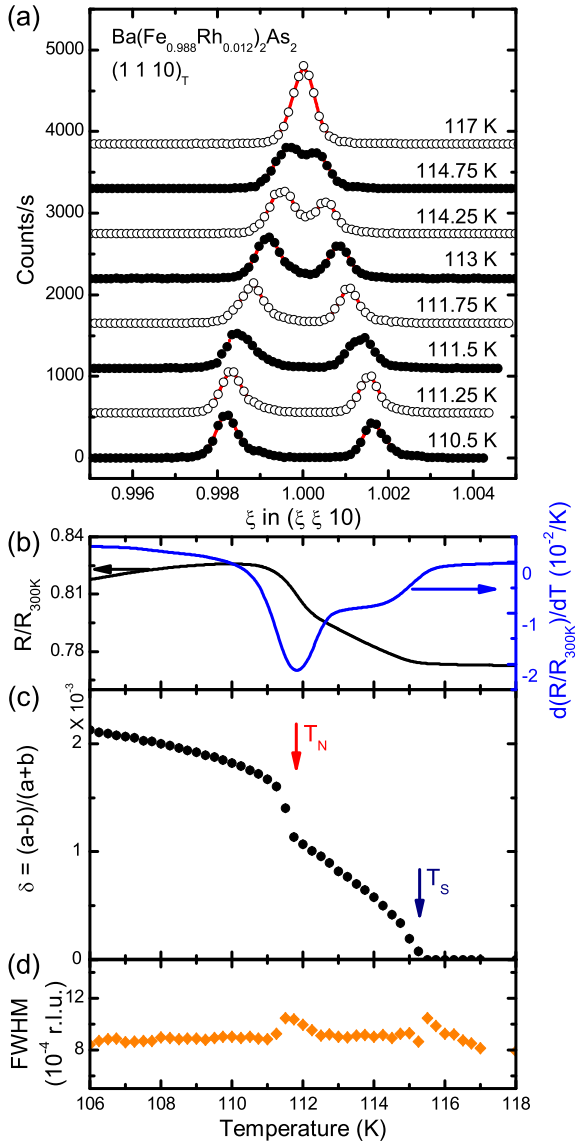

FIG. 4: (Color online) (a) X-ray data, (b) resistance (black line) and its temperature derivative (blue line), (c) orthorhombic distortion and (d) FWHM of the split $(1\ 1\ 10)_T$ Bragg peaks measured for $Ba(Fe_{1-x}Rh_x)_2As_2$ with $x = 0.012$. In panel (c) the structural and magnetic transition temperatures are marked.

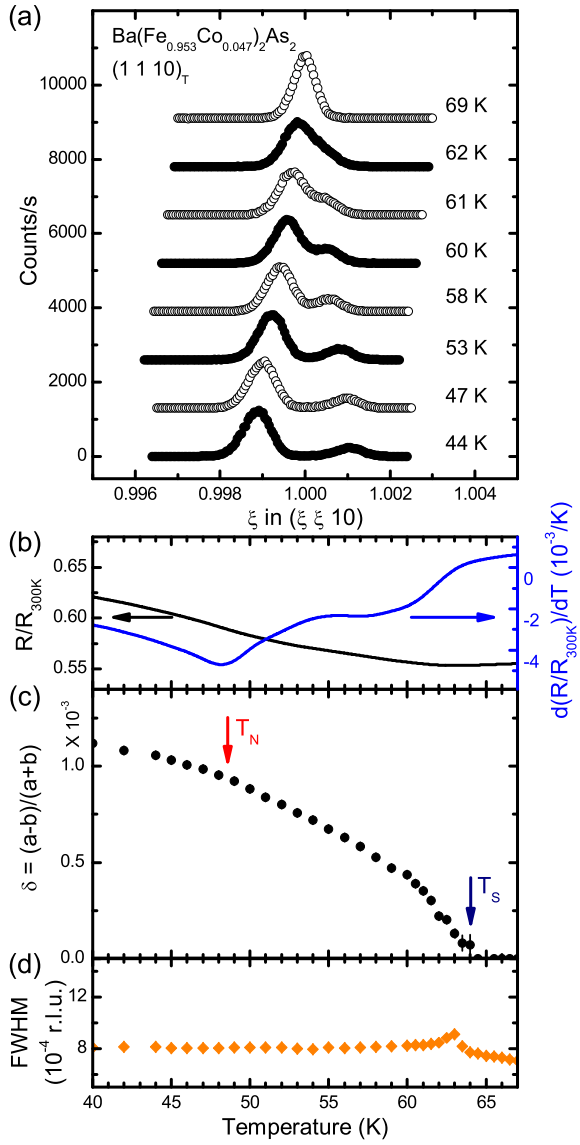

FIG. 5: (Color online) (a) X-ray data, (b) resistance (black line) and its temperature derivative (blue line), (c) orthorhombic distortion and (d) FWHM of the split $(1\ 1\ 10)_T$ Bragg peaks measured for $Ba(Fe_{1-x}Co_x)_2As_2$ with $x = 0.047$. In panel (c) the structural and magnetic transition temperatures are marked.

the data, and the electrical resistance measured as a function of temperature.

Turning first to the compounds at lower doping concentrations, $Ba(Fe_{0.982}Co_{0.018})_2As_2$ and $Ba(Fe_{0.988}Rh_{0.012})_2As_2$ (Figs. 3 and 4), below T_S both samples manifest a lattice distortion that evolves continuously as temperature is lowered, until the onset of magnetic ordering where a step-like feature in the structural order parameter (δ) is observed. At T_N a distinct broadening of the split orthorhombic diffraction peaks is evident over a narrow range in temperature. In contrast, the temperature dependence of the order parameter and peak widths for the higher doping concentrations, $Ba(Fe_{0.953}Co_{0.047})_2As_2$ and $Ba(Fe_{0.960}Rh_{0.040})_2As_2$, is decidedly different near T_N (Figs. 5 and 6). For these samples, the structural distortion evolves continuously, with only a mild kink in evidence at T_N and without the attendant peak broadening at T_N.

The differences between the lower and higher doping concentrations are consistent with a change in the nature of the magnetic transition from first-order for low doping, to second-order for higher doping levels. At low-doping, as for the parent $BaFe_2As_2$ compound, there is a second-order transition from the tetragonal phase to the Ort-PM structure as temperature is decreased below T_S. The step in the orthorhombic

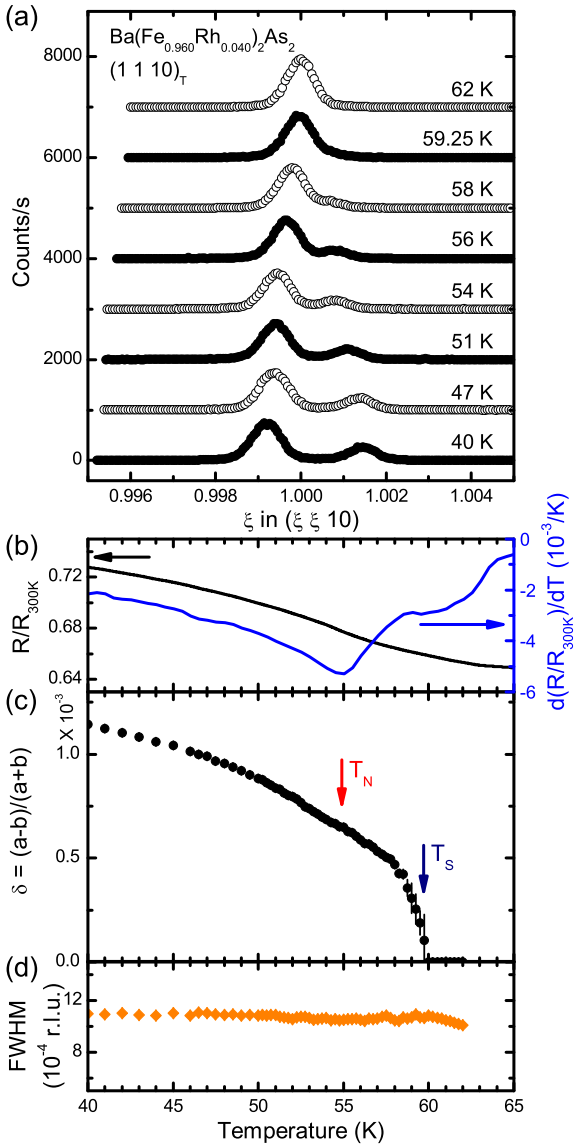

FIG. 6: (Color online) (a) X-ray data, (b) resistance (black line) and its temperature derivative (blue line), (c) orthorhombic distortion and (d) FWHM of the split $(1\ 1\ 10)_T$ Bragg peaks measured for $Ba(Fe_{1-x}Rh_x)_2As_2$ with $x = 0.040$. In panel (c) the structural and magnetic transition temperatures are marked.

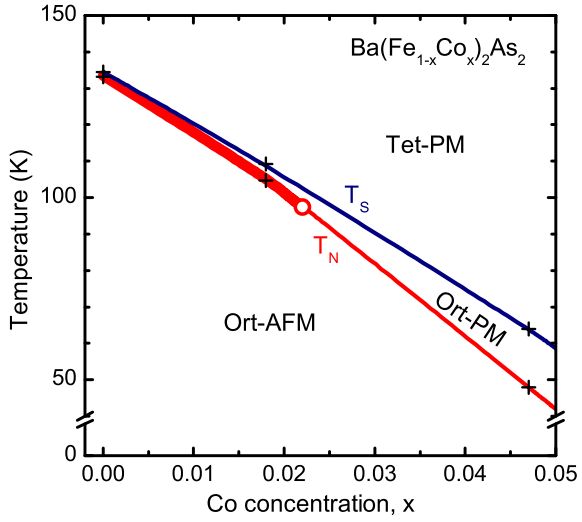

FIG. 7: (Color online) Diagram showing the nature of the structural and magnetic phase transitions for $Ba(Fe_{1-x}Co_x)_2As_2$ at T_S and T_N, respectively. The thick line denotes a first-order transition whereas the thinner lines represent second-order transitions. The crosses denote values for T_S and T_N determined from our measurements. The open circle denotes the approximate position of a tricritical point as described in the text.

distortion (δ) at T_N is a consequence of the abrupt appearance of Ort-AFM coincident with a first-order AFM transition. We note that throughout this temperature range only two broadened peaks are observed in contrast to what was shown above for the parent compound. This is expected, however, since the larger separation of T_S and T_N allows δ to evolve to a value for the Ort-PM phase that is close to its magnitude for the Ort-AFM phase. The anomalous increase in the widths of the x-ray diffraction peaks at T_N arises from the coexistence and near coincidence in position of the Ort-AFM and Ort-PM diffraction peaks over a narrow temperature range. For the higher doping levels, within our experimental resolution, the absence of a distinct step in δ or peak broadening at T_N is consistent with second-order AFM and structural transitions as found for electron-doped $BaFe_2As_2$ previously.[23,24]

We summarize our results in Fig. 7 which displays a phase diagram for $Ba(Fe_{1-x}Co_x)_2As_2$ focusing on the concentration range of the present study. The structural transition, over the entire range is second-order, whereas the magnetic transition changes from first-order to second-order at a tricritical point as discussed below.

IV. DISCUSSION

To understand the existence, and estimate the location, of a magnetic tricritical point in the phase diagram of $Ba\,(Fe_{1-x}Co_x)_2\,As_2$, we can, at first, rationalize the interplay between the magnetic and elastic degrees of freedom in terms of a simple Ginzburg-Landau model, similar to what was done by Cano *et al.* in Ref. 33. We start from the effective free energy:

$$F_{\rm eff} = \left(\frac{a_\delta}{2}\delta^2 + \frac{u_\delta}{4}\delta^4\right) + \left(\frac{a_m}{2}m^2 + \frac{u_m}{4}m^4\right) - \lambda\delta\, m^2 \quad (1)$$

with $a_\delta = a_{\delta,0}\,(T - T_{S,0})$, $a_m = a_{m,0}\,(T - T_{N,0})$, and positive constants u_δ, u_m, λ. Here, m is the antiferromagnetic order parameter and $T_{S,0}$, $T_{N,0}$ denote the bare structural and magnetic transition temperatures respectively. For $T_{S,0} < T_{N,0}$, this model describes a simultaneous magnetic/structural first-order transition. However, for $T_{S,0} > T_{N,0}$, this model describes a second-order structural transition at $T_S = T_{S,0}$, followed by a magnetic transition at

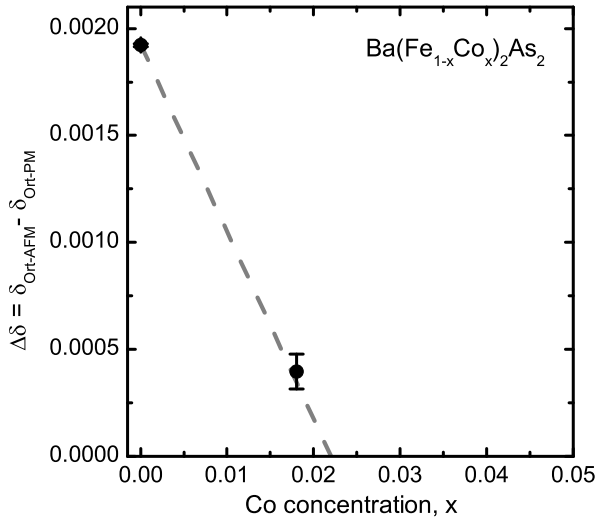

FIG. 8: Jump of the orthorhombic order parameter $\Delta\delta \equiv \delta_{\mathrm{Ort-AFM}} - \delta_{\mathrm{Ort-PM}}$ across the first-order magnetic transition, as function of x. The linear relationship $\Delta\delta \propto (x - x_{\mathrm{tri}})$ (dashed line) follows from the mean-field solution of Eq. 1.

T_N ($T_{N,0} < T_N < T_S$), which can be either first-order or second-order. Considering that T_N and T_S change with doping, the magnetic tricritical point takes place at the doping concentration x_{tri} where $u_m a_{\delta,0} (T_S - T_N) = \lambda^2$. Experimentally, we know that $(T_S - T_N)$ increases with doping, x. Therefore, it is straightforward to conclude from the mean-field solution of Eq. (1) that, close to the magnetic tricritical point, the jump in the orthorhombic order parameter across the first-order magnetic transition changes with doping as $\Delta\delta \equiv \delta_{\mathrm{Ort-AFM}} - \delta_{\mathrm{Ort-PM}} \propto (x - x_{\mathrm{tri}})$. Extrapolating this linear relation and using the values of $\Delta\delta$ from Figs. 1 and 3, we estimate that the magnetic tricritical point is located at $x_{\mathrm{tri}} \approx 0.022$, as shown in Fig. 8.

The main issue with the model in Eq. (1), however, is that it requires a fine tuning of the independent structural and magnetic transition temperatures $T_{S,0}$ and $T_{N,0}$ across the phase diagram. In all of the phase diagrams of the iron pnictide compounds, it is observed that the two transition lines track each other very closely, even within the superconducting dome.[23,34] This suggests that these two states are strongly coupled, rather than independent, as assumed by the previous model. To address this issue, it has been proposed that the particular magnetic structure of the iron pnictides gives rise to emergent Ising-nematic degrees of freedom that couple to the lattice, inducing the tetragonal-to-orthorhombic phase transition.[34–36] In the magnetically ordered phase, there are two degenerate ground states characterized by in-plane spin stripes along each of the two orthogonal Fe-Fe bond directions. These ground states can be described in terms of two interpenetrating AFM sublattices with staggered magnetization $\mathbf{m}_1$ and $\mathbf{m}_2$, such that $\mathbf{m}_1$ is either parallel or antiparallel to $\mathbf{m}_2$ (see Fig. 9).

Within this description, the magnetic free energy of the system F_{mag} has contributions from each sublattice F_i and from the coupling between them, F_{12}. The former is given by:

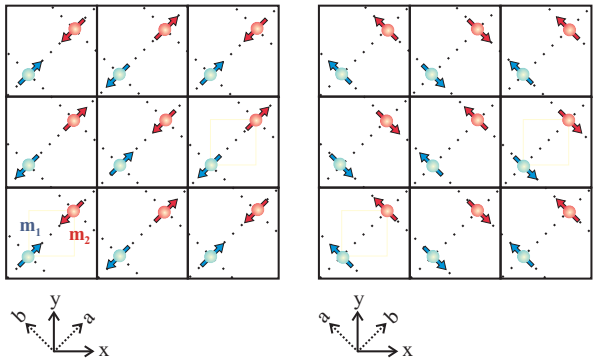

FIG. 9: (Color online) The two magnetic ground states of the iron pnictides, characterized by stripes along two orthogonal directions, expressed in terms of two interpenetrating AFM sublattices with Néel vectors $\mathbf{m}_1$ and $\mathbf{m}_2$. Notice that the (x, y) coordinate system used here refers to the unit cell with two Fe atoms and is rotated by 45° with respect to the (a, b) coordinate system relative to the single-Fe atom unit cell.

$$F_i = \frac{1}{2}\int \frac{d^3q}{(2\pi)^3}\, \chi_i^{-1}(\mathbf{q})\, \mathbf{m}_i(\mathbf{q}) \cdot \mathbf{m}_i(-\mathbf{q}) + \frac{u}{4}\int \frac{d^3x}{v}\, \mathbf{m}_i^4 \tag{2}$$

where $\chi_i(\mathbf{q}) = \chi_0 \left(r_0 + q_{\parallel}^2 a^2 - 2\eta_z \cos q_{\perp} c\right)^{-1}$ is the static susceptibility of each sublattice,[34] u is a positive coupling constant, and the momentum $\mathbf{q}$ is measured relative to the magnetic ordering vector. Here, χ_0^{-1} is a magnetic energy scale, r_0 measures the distance to the magnetic critical point, a and c are the lattice parameters of the unit cell of volume v containing two Fe atoms, and η_z is the inter-plane AFM coupling. The coupling between the two sublattices is given by:

$$F_{12} = -\frac{g}{2}\int \frac{d^3x}{v}\, (\mathbf{m}_1 \cdot \mathbf{m}_2)^2 \tag{3}$$

with $g > 0$, favoring configurations where $\mathbf{m}_1$ and $\mathbf{m}_2$ are either parallel or antiparallel. In a description of the magnetically ordered phase in terms of localized moments, this term originates from quantum and thermal spin fluctuations.[37] On the other hand, within an itinerant approach, where the magnetic moments arise from the conduction electrons, the same term appears as a consequence of the ellipticity of the electron pockets.[38]

The coupling (3) between the sublattices gives rise to an emergent Ising-nematic degree of freedom $\varphi = \mathbf{m}_1 \cdot \mathbf{m}_2$,[37] which may be finite even in the absence of magnetic order (i.e. $\langle\varphi\rangle \neq 0$, but $\langle\mathbf{m}_i\rangle = 0$) as long as the magnetic fluctuations are strong enough.[34] A finite value, $\langle\mathbf{m}_1 \cdot \mathbf{m}_2\rangle \neq 0$, breaks the Ising symmetry embedded in Eq. (3) and, consequently, the tetragonal symmetry. This can be seen explicitly through the magneto-elastic term:

$$F_{\mathrm{mag-el}} = \lambda \int \frac{d^3x}{v}\, \delta(\mathbf{m}_1 \cdot \mathbf{m}_2) \tag{4}$$

where $\lambda > 0$ is the magneto-elastic coupling and δ is the orthorhombic distortion. From the bilinear coupling of δ and φ in Eq. (4), both the nematic and structural transitions are simultaneous. This mechanism for the tetragonal-to-orthorhombic transition explains why the magnetic and structural transitions track each other closely in all the phase diagrams of the iron pnictides. Furthermore, it also explains several experimental observations, such as the softening of the lattice in the tetragonal phase and its hardening in the superconducting state,[34] as well as the suppression of the orthorhombic distortion below the superconducting transition temperature.[23]

In the case where the elastic free energy is harmonic, $F_{el} = C_s\delta^2/2$ [where C_s is the shear modulus] the only effect of the elastic degree of freedom is to renormalize the sublattice coupling constant g in Eq. (3), yielding $g \to g + \lambda^2/C_s$.[34] In a mean-field approach, this implies that the two transitions remain split and second order. Although fluctuations could induce a simultaneous first-order transition,[39,40] it is unclear whether they could explain a second-order structural transition split from a first-order magnetic transition, as our data for low doping levels in $BaFe_2As_2$ suggests.

To account for our observations, we move beyond the harmonic lattice approximation to consider the effects of anharmonic elastic terms (for more details on the formalism, see Ref. 41). In the tetragonal phase, the most general form of the free energy can be written as $F_{\rm el} = \frac{1}{2}\bar{C}_{ij}\epsilon_i\epsilon_j + \frac{1}{6}\bar{C}_{ijk}\epsilon_i\epsilon_j\epsilon_k$, where $\bar{C}_{ij}$ are given in terms of the six independent elastic constants and the strain components ϵ_i are:

$$\begin{aligned} \epsilon_1 &= u_{xx} + u_{yy} + u_{zz} \quad ; \quad \epsilon_4 = 2u_{yz} \\ \epsilon_2 &= (u_{xx} + u_{yy} - 2u_{zz})/6 \quad ; \quad \epsilon_5 = 2u_{xz} \\ \epsilon_3 &= (u_{xx} - u_{yy})/\sqrt{2} \quad ; \quad \epsilon_6 = 2u_{xy} \end{aligned} \tag{5}$$

with $u_{ij} = (\partial_i u_j + \partial_j u_i)/2$ and $\mathbf{u} = (u_x, u_y, u_z)$ denoting the displacement vector. In this notation, we have the orthorhombic distortion $\delta = \epsilon_6/2$ and the shear modulus $C_s \equiv 4\bar{C}_{66}$. Since we are interested in describing the transition from the tetragonal to the orthorhombic phase, we retain only the essential anharmonic terms that contain ϵ_6:

$$\begin{aligned} F_{\rm el} = \frac{1}{2}\bar{C}_{11}\epsilon_1^2 + \frac{1}{2}\bar{C}_{22}\epsilon_2^2 + \bar{C}_{12}\epsilon_1\epsilon_2 + \frac{1}{2}\bar{C}_{44}\left(\epsilon_4^2+\epsilon_5^2\right) + \\ \frac{1}{2}\bar{C}_{66}\epsilon_6^2 + \frac{1}{2}\left[\bar{C}_{166}\epsilon_1 + \bar{C}_{266}\epsilon_2\right]\epsilon_6^2 + \bar{C}_{456}\epsilon_4\epsilon_5\epsilon_6 \end{aligned} \tag{6}$$

Minimization with respect to the other strain components yields an effective elastic free energy in terms only of $\epsilon_6 = 2\delta$:

$$F_{\rm el}[\delta] = \frac{1}{2}C_s\delta^2 + \frac{1}{4}U\delta^4 + \frac{1}{6}W\delta^6 \tag{7}$$

where we included the sixth-order term $W > 0$ to ensure stability of the functional. Note that since:[41]

$$\frac{U}{16} = U_0 - \frac{\left(\bar{C}_{22}\bar{C}_{166}^2 - 2\bar{C}_{12}\bar{C}_{166}\bar{C}_{266} + \bar{C}_{11}\bar{C}_{266}^2\right)}{2\left(\bar{C}_{11}\bar{C}_{22} - \bar{C}_{12}^2\right)} \tag{8}$$

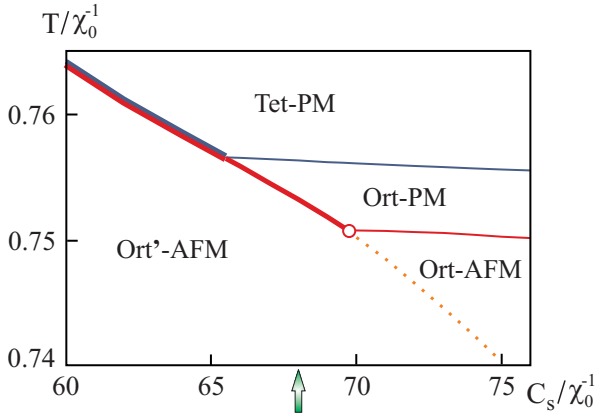

FIG. 10: (Color online) Phase diagram of the system with anharmonic elastic terms. T denotes temperature, C_s is the bare shear modulus, and χ_0^{-1} is a magnetic energy scale. Thin (thick) lines refer to second-order (first-order) phase transitions, with the red (blue) lines denoting magnetic (structural) transitions; the simultaneous first-order transition line is denoted by the double line. We use the notation Ort' to emphasize that the orthorhombic distortion jumps across the first-order magnetic transition. The orange dotted line signals the occurrence of a jump in both the magnetic and orthorhombic order parameters, without symmetry breaking. The open circle refers to the magnetic tricritical point, while the arrow indicates the value of C_s for which we calculate the temperature dependence of both the magnetic and orthorhombic order parameter (see Fig. 11).

the fourth-order coefficient can be negative, depending on the magnitudes of the anharmonic terms $\bar{C}_{ijk}$. Here, U_0 is the bare coefficient coming from higher-order quartic anharmonic terms.

In what follows, we consider all elastic coefficients to be temperature independent, and that the only minimum of Eq. (7) is at $\delta = 0$. Thus, different from the model in Eq. (1), the system has no intrinsic structural instability, and the elastic phase transition results solely from the magneto-elastic coupling in Eq. (4). In the case of a harmonic lattice, it was shown that nematic fluctuations renormalize the shear modulus in the tetragonal phase, making it vanish when the magnetic correlation length achieves a threshold value.[34] Here, not only C_s will be renormalized by nematic fluctuations, but also the anharmonic term U in Eq. (7), which gives rise to a much richer phase diagram.

To calculate the total free energy of the system, we use the 'mean-field $1/N$ approach' discussed elsewhere.[34,35] Basically, we assume that the magnetic order parameter $\mathbf{m}_i$ has N components and expand to leading order for large N. We then obtain self-consistent equations involving the magnetic correlation length ξ, the nematic order parameter φ, the magnetic order parameter $m = |\langle\mathbf{m}_1\rangle| = |\langle\mathbf{m}_2\rangle|$, and the orthorhombic distortion δ. The latter is obtained by minimizing the effective elastic free energy $F_{\rm eff} = F_{\rm el} + \tilde{F}$, where $\tilde{F}$ is an implicit function of δ, arising from the $1/N$ solution of the magnetic problem with free energy $F_{\rm mag} + F_{\rm mag-el}$. Thus, $\tilde{F}$ describes how magnetism changes the elastic free energy.

We choose parameters that yield relative temperatures and jumps comparable to those observed experimentally (see Sec-

tion IIIB).[42] In particular, we take $U < 0$ in Eq. (7); once again, we stress that the values used for U do not introduce any local minimum other than $\delta = 0$ in the bare F_{el}. To illustrate the richness of the resulting phase diagram, in Fig. 10 we show the results obtained after fixing all parameters but the bare shear modulus C_s. For smaller values of C_s, the system undergoes a simultaneous first-order structural/magnetic transition from the tetragonal/paramagnetic phase to the orthorhombic/antiferromagnetic phase. This corresponds to a direct first-order transition from the Tet-PM phase to the Ort-AFM phase, which has not been observed in the experiments reported here.

As the bare shear modulus increases, the two transitions split: at higher temperatures, the system undergoes a *second-order* structural transition and then a *first-order* magnetic transition at lower temperature. The latter is accompanied by a discontinuity in the orthorhombic order parameter δ due to the magneto-elastic coupling. This is precisely the sequence observed in our experiments described in Section III for the parent $BaFe_2As_2$ and doped compounds for low doping concentrations (Tet-PM $\rightarrow$ Ort-PM $\rightarrow$ Ort-AFM). Note that this is not another structural phase transition, but a consequence of the first-order character of the magnetic transition. To show this explicitly, in Fig. 11, we plot both δ and m as function of temperature for the value of C_s indicated by the arrow in Fig. 10. Not only is the relative size of the step comparable to that measured experimentally for $BaFe_2As_2$, but also the relative temperature at which the step occurs (see Fig. 1(b), where $T_s \approx 134.6$ K and $T_N \approx 134$ K). The discontinuity in the orthorhombic distortion accompanying the first-order magnetic transition is a very general feature that holds regardless of the specific values of the parameters. Thus, it supports our interpretation that the experimental data in Fig. 1 on the parent compound, $BaFe_2As_2$, describe a second-order structural transition followed by a first-order magnetic transition.

Returning to the phase diagram of Fig. 10, we note that as the shear modulus is increased even further, the transitions remain split but the magnetic transition becomes second-order, as it is observed for higher doping concentrations in $Ba(Fe_{1-x}Co_x)_2As_2$ and $Ba(Fe_{1-x}Rh_x)_2As_2$. At low temperatures, there is another line that marks a simultaneous jump in both the magnetic and the orthorhombic order parameter, without any symmetry breaking. However, we point out that in our $1/N$ approach we have not taken into account a key feature of the magnetically ordered state: the reconstruction of the Fermi surface. For instance, we note that $x_{\rm tri} \approx 0.02$ is close to the composition where evidence for a Lifshitz transition, below T_N, in $Ba(Fe_{1-x}Co_x)_2As_2$ has been reported by thermoelectric power, Hall coefficient measurements and angle-resolved photoemission.[43,44] Therefore, features in our model deep in the magnetically ordered phase, such as this extended line, are likely to change once the reconstruction of the Fermi surface is considered. For instance, one possibility is that this extended line terminates at a finite temperature critical point.

Furthermore, although in the phase diagram of Fig. 10 we changed only the bare shear modulus, it is unlikely that this is the only modified parameter as doping is introduced in the parent compound. In particular, the increase in the splitting between the transitions is much more modest in Fig. 10 than found experimentally (Fig. 7). It is possible, then, that other parameters controlling the splitting are also changed, such as the magneto-elastic coupling, λ, and the inter-plane magnetic coupling, η_z. The main objective of the phase diagram presented here is to illustrate the various possible phase transitions once anharmonic elastic terms are taken into account. It is interesting to note that, in our simple phase diagram, systems with softer lattices are more likely to display simultaneous first-order transitions. Indeed, $CaFe_2As_2$, which is significantly softer than $BaFe_2As_2$, presents relatively strong simultaneous first-order transitions.[5]

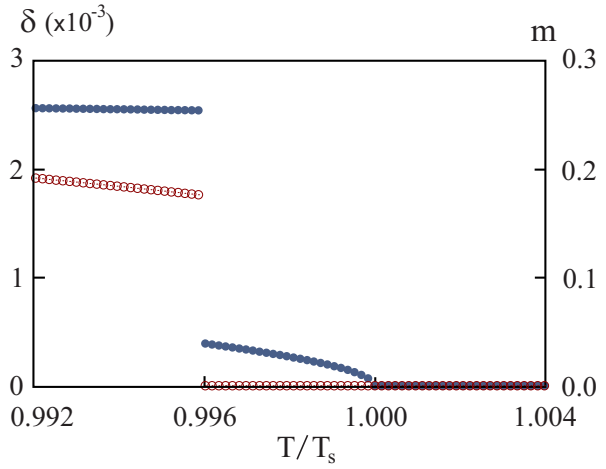

FIG. 11: (Color online) Magnetic (m, open symbols) and orthorhombic (δ, filled symbols) order parameters as function of temperature T (in units of the structural transition temperature T_s) for the system indicated by the green arrow in the phase diagram of Fig. 10.

V. SUMMARY

Our high-resolution x-ray diffraction and XRMS studies of $BaFe_2As_2$ have provided several new insights concerning the nature of the structural and magnetic transitions in the fascinating *122* iron pnictide family. First, we find that the orthorhombic distortion at T_S is best described as a second-order transition and that the structural and AFM transitions in the as-grown $BaFe_2As_2$ compound are separated in temperature by approximately 0.75 K. We propose that a first-order magnetic transition at T_N drives the discontinuity in the structural order parameter at 133.75 K, and this is consistent with our measurements of the evolution of the character of the transitions in Co- and Rh-doped $BaFe_2As_2$. Using these results, we can provide an estimate of the position of a tricritical point in the phase diagram of $Ba(Fe_{1-x}Co_x)_2As_2$. Finally, we employ a mean-field approach to show that our measurements can be explained by the inclusion of an anharmonic term in the elastic free energy and magneto-elastic coupling in the form of an emergent Ising-nematic degree of freedom.

We acknowledge valuable discussions with J. Lang. This

work was supported by the Division of Materials Sciences and Engineering, Office of Basic Energy Sciences, U.S. Department of Energy. Ames Laboratory is operated for the U.S. Department of Energy by Iowa State University under Contract No. DE-AC02-07CH11358. Use of the Advanced Photon Source was supported by the US DOE under Contract No. DE-AC02-06CH11357.

[1] Y. Kamihara, T. Watanabe, M. Hirano, and H. Hosono, J. Am. Chem. Soc. **130**, 3296 (2008).
[2] M. Rotter, M. Tegel, and D. Johrendt, Phys. Rev. Lett. **101**, 107006 (2008).
[3] M. D. Lumsden and A. D. Christianson, J. Phys.: Condens. Matter **22**, 203203 (2010).
[4] M. Rotter, M. Tegel, D. Johrendt, I. Schellenberg, W. Hermes, and R. Pöttgen, Phys. Rev. B **78**, 020503 (2008).
[5] A. I. Goldman, D. N. Argyriou, B. Ouladdiaf, T. Chatterji, A. Kreyssig, S. Nandi, N. Ni, S. L. Bud'ko, P. C. Canfield, and R. J. McQueeney, Phys. Rev. B **78**, 100506(R) (2008).
[6] J. Yan, A. Kreyssig, S. Nandi, N. Ni, S. L. Bud'ko, A. Kracher, R. J. McQueeney, R. W. McCallum, T. A. Lograsso, A. I. Goldman, et al., Phys. Rev. B **78**, 024516 (2008).
[7] J. Zhao, W. Ratcliff, J. W. Lynn, G. F. Chen, J. L. Luo, N. L. Wang, J. Hu, and P. Dai, Phys. Rev. B **78**, 140504(R) (2008).
[8] A. Jesche, N. Caroca-Canales, H. Rosner, H. Borrmann, A. Ormeci, D. Kasinathan, H. H. Klauss, H. Luetkens, R. Khasanov, A. Amato, et al., Phys. Rev. B **78**, 180504 (2008).
[9] Q. Huang, Y. Qiu, W. Bao, M. A. Green, J. W. Lynn, Y. C. Gasparovic, T. Wu, G. Wu, and X. H. Chen, Phys. Rev. Lett. **101**, 257003 (2008).
[10] P. C. Canfield and S. L. Bud'ko, Annu. Rev. Condens. Matter Phys. **1**, 27 (2010).
[11] N. Ni, M. E. Tillman, J. Yan, A. Kracher, S. T. Hannahs, S. L. Bud'ko, and P. C. Canfield, Phys. Rev. B **78**, 214515 (2008).
[12] J.-H. Chu, J. G. Analytis, C. Kucharczyk, and I. R. Fisher, Phys. Rev. B **79**, 014506 (2009).
[13] L. J. Li, Y. K. Luo, Q. B. Wang, H. Chen, Z. Ren, Q. Tao, Y. K. Li, X. Lin, M. He, Z. W. Zhu, et al., New J. Phys. **11**, 025008 (2009).
[14] C. Lester, J.-H. Chu, J. G. Analytis, S. C. Capelli, A. S. Erickson, C. L. Condron, M. F. Toney, I. R. Fisher, and S. M. Hayden, Phys. Rev. B **79**, 144523 (2009).
[15] D. K. Pratt, W. Tian, A. Kreyssig, J. L. Zarestky, S. Nandi, N. Ni, S. L. Bud'ko, P. C. Canfield, A. I. Goldman, and R. J. McQueeney, Phys. Rev. Lett. **103**, 087001 (2009).
[16] A. D. Christianson, M. D. Lumsden, S. E. Nagler, G. J. MacDougall, M. A. McGuire, A. S. Sefat, R. Jin, B. C. Sales, and D. Mandrus, Phys. Rev. Lett. **103**, 087002 (2009).
[17] A. Kreyssig, M. G. Kim, S. Nandi, D. K. Pratt, W. Tian, J. L. Zarestky, N. Ni, A. Thaler, S. L. Bud'ko, P. C. Canfield, et al., Phys. Rev. B **81**, 134512 (2010).
[18] M. Wang, H. Luo, J. Zhao, C. Zhang, M. Wang, K. Marty, S. Chi, J. W. Lynn, A. Schneidewind, S. Li, et al., Phys. Rev. B **81**, 174524 (2010).
[19] H. Chen, Y. Ren, Y. Qiu, W. Bao, R. H. Liu, G. Wu, T. Wu, Y. L. Xie, X. F. Wang, Q. Huang, et al., Europhys. Lett. **85**, 17006 (2009).
[20] S. Jiang, H. Xing, G. Xuan, C. Wang, Z. Ren, C. Feng, J. Dai, Z. Xu, and G. Cao, J. Phys.: Condens. Matter **21**, 382203 (2009).
[21] A. Thaler, N. Ni, A. Kracher, J. Q. Yan, S. L. Bud'ko, and P. C. Canfield, Phys. Rev. B **82**, 014534 (2010).
[22] M. G. Kim, D. K. Pratt, G. E. Rustan, W. Tian, J. L. Zarestky, A. Thaler, S. L. Bud'ko, P. C. Canfield, R. J. McQueeney, A. Kreyssig, et al., Phys. Rev. B **83**, 054514 (2011).
[23] S. Nandi, M. G. Kim, A. Kreyssig, R. M. Fernandes, D. K. Pratt, A. Thaler, N. Ni, S. L. Bud'ko, P. C. Canfield, J. Schmalian, et al., Phys. Rev. Lett. **104**, 057006 (2010).
[24] R. M. Fernandes, D. K. Pratt, W. Tian, J. Zarestky, A. Kreyssig, S. Nandi, M. G. Kim, A. Thaler, N. Ni, P. C. Canfield, et al., Phys. Rev. B **81**, 140501(R) (2010).
[25] K. Kitagawa, N. Katayama, K. Ohgushi, and M. Takigawa, J. Phys. Soc. Jpn. **78**, 063706 (2009).
[26] K. Matan, R. Morinaga, K. Iida, and T. J. Sato, Phys. Rev. B **79**, 054526 (2009).
[27] M. Kofu, Y. Qiu, W. Bao, S. Lee, S. Chang, T. Wu, G. Wu, and X. H. Chen, New J. Phys. **11**, 055001 (2009).
[28] K. Kitagawa, N. Katayama, K. Ohgushi, M. Yoshida, and M. Takigawa, J. Phys. Soc. Jpn. **77**, 114709 (2008).
[29] S. D. Wilson, Z. Yamani, C. R. Rotundu, B. Freelon, E. Bourret-Courchesne, and R. J. Birgeneau, Phys. Rev. B **79**, 184519 (2009).
[30] S. D. Wilson, C. R. Rotundu, Z. Yamani, P. N. Valdivia, B. Freelon, E. Bourret-Courchesne, and R. J. Birgeneau, Phys. Rev. B **81**, 014501 (2010).
[31] C. R. Rotundu, B. Freelon, T. R. Forrest, S. D. Wilson, P. N. Valdivia, G. Pinuellas, A. Kim, J. W. Kim, Z. Islam, E. Bourret-Courchesne, et al., Phys. Rev. B **82**, 144525 (2010).
[32] M. G. Kim, A. Kreyssig, Y. B. Lee, J. W. Kim, D. K. Pratt, A. Thaler, S. L. Bud'ko, P. C. Canfield, B. N. Harmon, R. J. McQueeney, et al., Phys. Rev. B **82**, 180412(R) (2010).
[33] A. Cano, M. Civelli, I. Eremin, and I. Paul, Phys. Rev. B **82**, 020408(R) (2010).
[34] R. M. Fernandes, L. H. VanBebber, S. Bhattacharya, P. Chandra, V. Keppens, D. Mandrus, M. A. McGuire, B. C. Sales, A. S. Sefat, and J. Schmalian, Phys. Rev. Lett. **105**, 157003 (2010).
[35] C. Fang, H. Yao, W.-F. Tsai, J. P. Hu, and S. A. Kivelson, Phys. Rev. B **77**, 224509 (2008).
[36] C. Xu, M. Müller, and S. Sachdev, Phys. Rev. B **78**, 020501(R) (2008).
[37] P. Chandra, P. Coleman, and A. I. Larkin, Phys. Rev. Lett. **64**, 88 (1990).
[38] I. Eremin and A. V. Chubukov, Phys. Rev. B **81**, 024511 (2010).
[39] V. Barzykin and L. P. Gor'kov, Phys. Rev. B **79**, 134510 (2009).
[40] Y. Qi and C. Xu, Phys. Rev. B **80**, 094402 (2009).
[41] G. Fadda, L. Truskinovsky, and G. Zanzotto, Phys. Rev. B **66**, 174107 (2002).
[42] We use the parameters $\eta_z = 2 \times 10^{-3}$, $\lambda = 0.3\chi_0^{-1}$, $U \approx -2 \times 10^7 \chi_0^{-1}$, and $W \approx 2 \times 10^{12}\chi_0^{-1}$. The relative orders of magnitude between $C_s \sim 10^2\chi_0^{-1}$, U, and W are associated with the equilibrium value of the orthorhombic distortion, $\delta \sim 10^{-3}$.
[43] E. D. Mun, S. L. Bud'ko, N. Ni, A. N. Thaler, and P. C. Canfield, Phys. Rev. B **80**, 054517 (2009).
[44] C. Liu, T. Kondo, R. M. Fernandes, A. D. Palczewski, E. D. Mun, N. Ni, A. N. Thaler, A. Bostwick, E. Rotenberg, J. Schmalian, et al., Nature Physics **6**, 419 (2010).